Presented at the WCPEC-8, 8th World Conference on Photovoltaic Energy Conversion, 26-30 September 2022, Milan, Italy

INFLUENCE OF IR SOLDERING PROFILE ON INDUSTRIAL SILICON HETEROJUNCTION SOLAR CELLS

Angela De Rose, Cristina Rosado Alberdi, Achim Kraft

Fraunhofer Institute for Solar Energy Systems ISE
Heidenhofstraße 2, 79110 Freiburg i.Br., Germany

*Corresponding author, e-mail to: angela.de.rose@ise.fraunhofer.de

ABSTRACT: Within this work, the influence of infrared (IR) light on bifacial *n*-type silicon heterojunction (SHJ) solar cells is investigated, with the focus on the industrial IR soldering process. The EL images and *I-V* parameters of industrial SHJ cells are compared before and after treatment with IR light. The temperature-time-profile of this thermal treatment is varied according to established soldering profiles used in silicon photovoltaics, reaching peak temperatures above 200 °C. As a result, a reliable process window for the interconnection process of SHJ solar cells is identified (max. 250 °C, max. 6 s), where thermal degradation is avoided and even slight improvements of the cell performance are observed (ΔV_{oc} = +1.9 mV, ΔFF = +0.3 %, $\Delta\eta$ = +0.1 %). Overall, these investigations demonstrate the feasibility of the established IR soldering process for SHJ solar cells during module integration and therefore extend the range of usable process options for a broad deployment of SHJ modules.
Keywords: silicon heterojunction (SHJ), temperature, soldering, interconnection, infrared light

1 INTRODUCTION

For the interconnection of silicon heterojunction (SHJ) solar cells, several challenges have to be faced, as reported by different groups [1–5]. Previous work has shown that reliable and damage-free infrared (IR) soldering can be used to interconnect SHJ solar cells and build full size solar modules [4]. Today, commercially available SHJ modules on the marked use both options, multi-wire interconnection and soldering flat ribbons [6]. All of them use process temperatures between 200 °C and 250 °C for interconnection. Beside a precise alignment of ribbon/wire and busbars/pads, the success of the soldering result strongly depends on the used temperatures within the whole production chain.

Due to their temperature sensitivity, the excellent passivation of the hydrogenated amorphous silicon (*a*-Si:H) layer of the SHJ solar cell could be damaged at high temperatures [7]. In addition, a too high thermal budget leads to an increase of the contact resistance at the heterojunction [8]. Hence, during cell processing, low-temperature processes are used for *e.g.* deposition of the *a*-Si layers (~200 °C) [5, 9], sputtering of the transparent conductive oxide (< 210 °C) [10, 11], and curing of the metallization (< 240 °C) [12, 13]. Also, additional annealing steps and light soaking during solar cell manufacturing have shown to be beneficial for the performance [14, 15]. Different SHJ cell manufacturer use slightly different temperatures, materials and cell thicknesses to optimize their cell technology. Therefore, the soldering process has to be adapted carefully, for a given fabrication sequence or cell supplier.

Within this work, the power of the IR radiator is varied to consequently change the peak temperature of the soldering profile between 200 °C and 320 °C, and the effect on the *I-V* parameters of industrial SHJ solar cells is evaluated. To optimize the whole process chain for production of SHJ solar modules, the effects of IR light and cell temperature have to be evaluated. The aim of this work is to find a reliable process window for IR soldering while minimizing the process time to ensure a high throughput for industrial manufacturing.

2 EXPERIMENTAL

To define a suitable temperature range for soldering SHJ solar cells, the influence of IR light on the SHJ cell has been studied by a systematic temperature variation during IR light treatment and selected solar cell characterization.

2.1 Infrared light treatment

A semi-automatic IR soldering station is used for thermal treatment of the industrial SHJ solar cells (*n*-type, monocrystalline, 156.75 mm × 156.75 mm, 5 busbars, bifacial, rear emitter). The experimental setup consists of an IR lamp (λ_{max} = 1.2 µm) and a hotplate with down-holding unit. One of the SHJ solar cells is used to develop and control the temperature profiles, given in Figure 1. For this, a thermocouple is placed in the center on the cell's front side beside the middle busbar. A hotplate is used for pre-heating to 120 ° C. After the alignment of SHJ cell and down holder on the hotplate, the IR treatment is performed, and the cell surface temperature is monitored against time.

Seven different temperature profiles are used. The peak temperature is varied between 200 °C and 320 °C with ΔT = 20 K, while the "soldering" time is kept constant at $t_s = t_{FWHM} \approx 6$ s. To reliably vary the peak temperature up to 320 °C and ensure comparable results, a constant soldering time t_s is used. Each variation is tested on N = 5 SHJ cells.

In addition to IR light, the influence of alternative heat sources on the SHJ cells are tested. To imitate contact soldering with a solder iron, a solder tip is used to locally induce heat into the cell metallization. Heat transfer by convection is tested with an oven at ambient air for different temperatures.

In addition to IR light, the influence of alternative heat sources on the SHJ cells are tested. To imitate contact soldering with a solder iron, a solder tip is used to locally induce heat into the cell metallization. Heat transfer by convection is tested with an oven at ambient air for different temperatures.

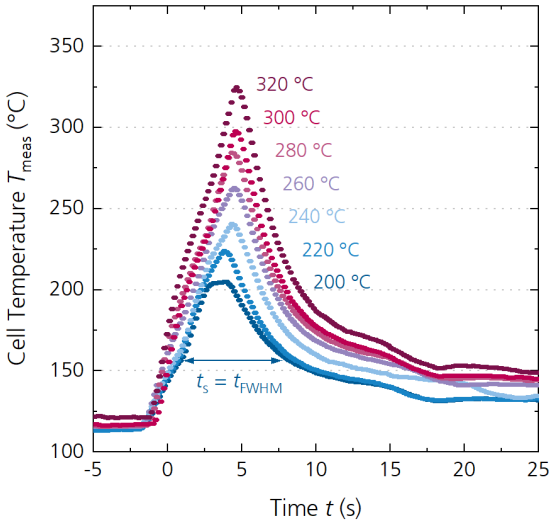

Figure 1: Measured solar cell temperature T_{meas} on the surface in the middle of an SHJ solar cell during IR treatment with different peak temperatures. The "soldering" time t_s is given by the full width at half maximum t_{FWHM} and kept constant.

During all heat treatments of the SHJ cells, no solder materials (*i.e.* solder alloy, flux) are used to focus on the effect of the IR treatment and eliminate other factors as *e.g.* possible material interactions.

2.2 Solar cell characterization

Solar cells are electrically characterized by electroluminescence (EL) imaging and *I-V* measurements, both before and after IR treatment of the cells. EL is done at 10 A. An inline *I-V* tester is used to measure the *I-V* curve under STC conditions. A reference group, consisting of five SHJ solar cells of the same batch, are used as measurement reference for EL and *I-V*. The systematic uncertainties (2σ) of the *I-V* measurements are: $\sigma_{Voc} = \pm 0.09$ %, $\sigma_{Isc} = \pm 0.15$ %, $\sigma_{FF} = \pm 0.17$ %, $\sigma_{pFF} = \pm 0.12$ %, $\sigma_{Pmpp} = \pm 1.62$ %, $\sigma_{\eta} = \pm 0.28$ %.

Selected samples are further characterized by Suns-V_{oc} measurements, using J_{sc} = 37 mA/cm^2, ρ_B = 4 Ω·cm and 165 µm cell thickness as input parameters, performing eight measurements per busbar.

2.3 Microscopic imaging

For high resolution imaging, scanning electron microscopy (SEM) is conducted in top view mode with 5 kV acceleration voltage, using an in-lens detector to measure the secondary electrons.

3 RESULTS AND DISCUSSION

In the following, the results of the IR light treatment of SHJ solar cells are presented. They are referred to a certain peak temperature, introduced during IR treatment. All qualitative and quantitative results are compared to the initial state of the cells before treatment.

3.1 Electrical characterization by EL and *I-V*

EL imaging is a fast and reliable method to detect defects (*e.g.* cracks, cell damage), introduced during cell interconnection. Therefore, we use EL images to evaluate possible local damage of the cells after the IR treatments.

Figure 2 exemplarily shows the EL images of one of the five solar cells for each peak temperature. The images are scaled to the same limits of the EL signal for better comparison. For a peak temperature of 260 °C and higher, local damage of the cell can be observed, indicated by a reduced EL signal (dark areas). These defect areas are more pronounced for higher temperatures. The position and exact shape of these spots strongly correlates to the arrangement of the IR radiators and the used downholding unit, both influencing the light propagation.

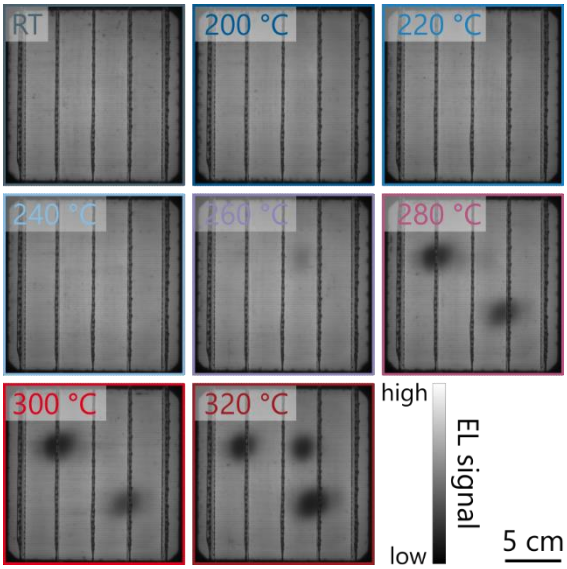

Figure 2: EL images of one example for each peak temperature, visualizing a local degradation for temperatures above ~260 °C.

To interconnect solar cells with a Sn60Pb40 solder alloy, peak temperatures of 230 °C – 240 °C have to be reached for a time of at least 1 s – 2 s. The EL images in Figure 2 let assume that no damage of the SHJ layers up to 240 °C for at least 6 s can be expected.

To quantify the damage of the SHJ cells for higher temperatures and define an upper limit for soldering, *I-V* measurements for all groups are performed. Figure 3 shows the open circuit voltage V_{oc} (top) and the fill factor *FF* and pseudo fill factor p*FF* (bottom) for the reference group, stored at room temperature (RT) and each peak temperature up to 320 °C.

By increasing the peak temperature up to 260 °C, a gain in V_{oc} of +(0.2 ± 0.1) % (absolute: +(1.9 ± 0.8) mV) is found. As reported by other researcher, investigating the impact of light soaking on SHJ solar cells, this is due to improved hydrogen passivation within the SHJ layers [15] and further healing of sputter damage. This shows that the soldering process could be used to further optimize the overall cell performance, when considering the whole production chain from cell to module.

After a certain threshold temperature is reached, the passivation and therefore V_{oc} degrades. Hydrogen effusion leads to depassivation and a local increase of the dark saturation current j_0 can be found [4]. Temperatures above 260 °C should be avoided during soldering to not damage the SHJ solar cell.

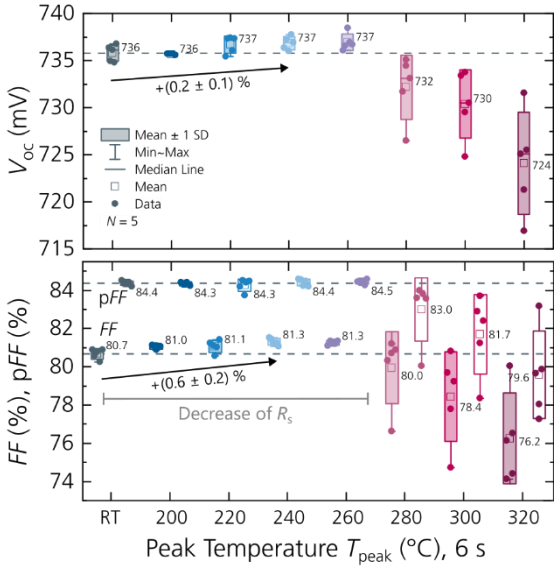

Figure 3: Open circuit voltage V_{oc}, fill factor *FF* and pseudo fill factor p*FF* of SHJ solar cells after IR treatment with different peak temperatures T_{peak} for a constant time of about 6 s. The horizontal dashed lines indicate the mean value of the reference group without treatment (RT = room temperature). Up to 260 °C, a gain in V_{oc} and *FF* is measured, whereas higher temperatures induce degradation of the SHJ solar cell.

The same trend is found for the fill factor *FF*, improving by +(0.6 ± 0.2) % (absolute: +(0.3 ± 0.1) %) for increased temperature up to 260 °C. In this temperature range, the pseudo fill factor p*FF* remains constant, whereas a decrease of the series resistance R_s is measured (not shown here), yielding to a boost in *FF*. The improvement of R_s can be attributed to post-curing of the metallization paste, which will be discussed in section 3.3.

Above 260 °C, p*FF* decreases as well, resulting in a decrease of *FF*. Here, several effects are overlapping: in addition to the decrease of R_s due to "post-curing", reduced charge carrier transport at the *a*-Si:H/TCO interface leads to a local increase of R_s [4, 8]. Since the overall change in Rs remains nearly constant (*cf.* Table 1), the decrease in p*FF* is dominated by local depassivation.

A summary of the change of the relevant *I-V* parameters is given in Table 1.

Table 1: Change of the *I-V* parameters, showing the mean change of *N* = 5 SHJ cells after the IR treatment with 240 °C for 6 s. The values are corrected by the *I-V* data of a control group of additional five SHJ cells (without IR treatment).

Parameter	Abs. change	Rel. change
V_{oc}	(1.9 ± 0.8) mV	(0.2 ± 0.1) %
J_{sc}	(0.0 ± 0.0) mA/cm^2	(0.0 ± 0.0) %
p*FF*	(0.1 ± 0.1) %	(0.1 ± 0.1) %
FF	(0.3 ± 0.1) %	(0.6 ± 0.2) %
R_s	(-0.03 ± 0.02) Ω·cm^2	(-10.2 ± 3.9) %
η	(0.10 ± 0.02) %	(0.7 ± 0.1) %

Similar overlapping effects, as described above, are found for the temperature around 260 °C. Here, the EL image already shows local depassivation (*cf.* Figure 2), whereas an overall gain of the *I-V* parameters (esp. V_{oc}, p*FF*, *FF*) is found (*cf.* Figure 3). These results show that global and spatial electrical analysis should be used complementary to provide a better understanding of the influence of IR soldering on SHJ solar cells.

3.3 SEM analysis of metallization

The IR light treatment does not only affect the layers of the SHJ cell structure, but also the metallization. The electrodes of the investigated cells consist of screen-printed and cured fingers and busbars, using an Ag low-temperature (LT) metallization paste. Figure 4 shows top view SEM images of the finger, before (left) and after IR light treatment with 340 °C peak temperature for 6 s (right, finger of degraded region).

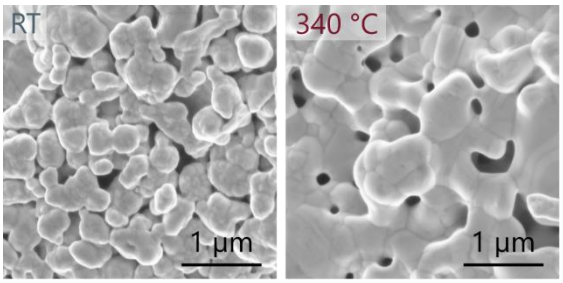

Figure 4: Top view SEM images of finger metallization (LT paste) of front side of industrial SHJ solar cell before (left) and after (right, degraded region) IR treatment with 340 °C for 6 s.

The IR light induces "post-curing" of the finger paste, leading to further sintering of the Ag particles. This results in a lower series resistance R_s, which causes an increase of the fill factor *FF* (*i.e.* Figure 3).

3.4 Local analysis of degradation by Suns-V_{oc}

By *I-V* measurements, mean electrical parameters of the whole SHJ solar cell are extracted. Local information over the wafer can be obtained by *e.g.* luminescence imaging. Another method to obtain local quantitative results for the quality of the cell is Suns-V_{oc}. One SHJ solar cell, treated with IR light at 340 °C for 6 s, is characterized by Suns-V_{oc}. The V_{oc}, determined by *I-V*, is 736 mV in the initial state and 706 mV in the degraded state after IR treatment, giving a loss of ΔV_{oc} = -30 mV.

Figure 5 shows the result of the Suns-V_{oc} measurement of this SHJ cell. The underlying EL image correlates well to the Suns-V_{oc} measurement. A maximum degradation of -75 mV is found at the position where the EL image shows the lowest signal. Also in the outer cell range, which seemed to be unaffected in the EL image, losses around 0.5 mV to 3 mV are observed.

The Suns-V_{oc} measurement confirms that the IR radiation leads to damage of the passivation layers, resulting in local degradation of up to ΔV_{oc} = -75 mV, correlating with a decrease in p*FF* (not shown here). In contrast, the V_{oc}, extracted from *I-V* measurements, only represents a mean value of the cell and is therefore less useful to qualify the damage. For the temperature range between 220 °C and 280 °C, these local changes play a major role; in this range, soldering is carried out. As electrical gains and losses are overlapping in this regime, as seen from our experiments, careful optimization is important.

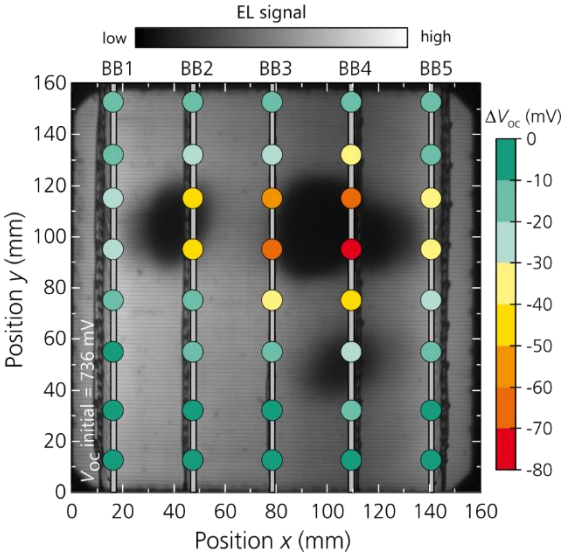

Figure 5: Suns-V_{oc} measurement of an SHJ solar cell after IR treatment for 6 s at 340 °C, correlated to its EL image. The measurement is performed at the marked positions along the five busbars.

3.4 Alternative heat sources for interconnection

Concerning SHJ solar cells, several annealing experiments have already been carried out, most of them using hotplates to control temperature and time precisely [7, 8, 10, 16]. However, for SHJ string and module production, other heat sources are more relevant. Therefore, we investigate the influence of different heat sources on the SHJ solar cells. Contact heat, as it is applied during contact soldering or lamination, convection heat induced by an oven or *e.g.* hot air soldering and, as reference, IR radiation. For each condition, an EL image after heat treatment is exemplarily shown in Figure 6.

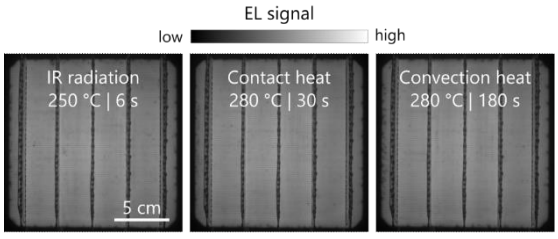

Figure 6: Influence of different soldering techniques (heat sources) on SHJ solar cells. For each technique, five SHJ cells are tested, whereas the temperature maximum T_{max}, tested for a time of t_{max} without inducing cell damage, is given. Both are set-parameters.

The aim of this variation is to identify a maximum thermal budget (temperature T_{max} for a certain time t_{max}), without inducing damage to the solar cell. The boundaries of these processes are identified using the same analysis by EL and *I-V* measurements as presented above, before and after thermal treatment. For all tested heat sources, the maximum suitable temperature is between 250 °C and 280 °C. The values for T_{max} and t_{max}, given in the EL images, refer to a maximum heat treatment, without degrading the electrical parameters of the cells (not shown here). Especially for IR radiation, one has to keep in mind the more inhomogeneous temperature distribution over the cell, compared to *e.g.* convection heating. Therefore, the given temperature of 250 °C can underestimate the local cell temperature in some regions.

For conventional soldering with Sn60Pb40, peak temperatures between 220 °C and 250 °C are used for soldering times < 2 s. During low-temperature soldering with Pb-free solder alloys, even lower temperatures < 220 °C are required [17]. Therefore, the identified values are far above the required temperatures and times for soldering solar cells.

Nevertheless, the maximum thermal budget of SHJ cells during module production has to be evaluated for each SHJ cell structure, since it is influenced by the thermal budget used during SHJ cell processing. However, a broad temperature range can be used for interconnection, allowing also peak temperatures up to 260 °C for 6 s (*e.g.* for IR soldering).

4 CONCLUSION AND OUTLOOK

In the past, studies have shown the high sensitivity of SHJ solar cells to elongated thermal treatment [7, 10]. Therefore, most work has taken a conservative approach and limiting the temperature range below 210 °C. Today, most processes have reached a high maturity and mass manufacturing is built up. Now, the limits of the thermal treatments have to be tested, to enable high throughput manufacturing.

In this work, we investigate the influence of different temperatures, induced by IR light, on industrial SHJ solar cells to identify a guideline for soldering of SHJ solar cells for manufacturing PV modules. Our evaluation shows no degradation of the SHJ solar cells after IR treatment for T_{max} < 260 °C and t_{max} = 6 s, as well tested for other heat sources (contact, convection). Indeed, the IR light causes a light soaking effect of the cell [15]. A slight gain of +0.2 % in V_{oc} and +0.6 % in *FF* is observed due to enhanced passivation quality and a post-curing of the metallization after IR treatment. SEM images of the finger metallization confirm further sintering of the Ag particles within the paste. These gains in cell performance could be further quantified after climate chamber testing of modules to proof the stability after further heat or light exposure.

For temperatures above ~260 °C for 6 s, local degradation can be observed by EL imaging and quantified by *I-V* measurements. Suns-V_{oc} measurements have shown to be suitable to identify local gains and losses in V_{oc}, also helpful to achieve homogenous solder joint formation over the cell. Since SHJ cells are sensitive to temperature and light, any small adjustment of the soldering process (*e.g.* temperature, belt speed, downholder *etc.*) can have a large influence on the soldering result and the SHJ cell. Furthermore, the temperatures given in this study, most probably underestimate the actual cell temperatures in the hottest regions during IR soldering. Therefore, the given thresholds (temperature, time) could also be understood as a lower limit for the onset of cell degradation.

During string production, EL imaging can be used as fast and reliable method to optimize the soldering result. However, the images must be evaluated quantitatively or directly correlated to *I-V* or Suns-V_{oc} measurements, since slight degradation may not be visible. These techniques are not jet implemented inline into module manufacturing lines before lamination, since a fast and damage-free transport of the strings is challenging.

Given the presence of further thermal treatments during module manufacturing, the whole process chain for SHJ should be optimized to enable the leanest fabrication path. This is focus of ongoing work at our institute.

5 REFERENCES

[1] A. Faes *et al.*, "Smartwire solar cell interconnection technology," in *Proceedings of the 29th European Photovoltaic Solar Energy Conference and Exhibition (EU PVSEC)*, Amsterdam, Netherlands, 2014, pp. 2555–2561.

[2] A. De Rose, T. Geipel, D. Erath, A. Kraft, and U. Eitner, "Challenges for the interconnection of crystalline silicon heterojunction solar cells," *Photovoltaics International*, vol. 40, pp. 78–86, 2018.

[3] C. Kaiser, V. Nikitina, T. Geipel, and A. Kraft, "Reduction of ECA amount for the ribbon interconnection of heterojunction solar cells," in *Proceedings of the 37th European Photovoltaic Solar Energy Conference and Exhibition (EU PVSEC)*, online, 2020, pp. 1086–1090.

[4] A. De Rose, T. Geipel, D. Eberlein, A. Kraft, and M. Nowottnick, "Interconnection of Silicon Heterojunction Solar Cells by Infrared Soldering - Solder Joint Analysis and Temperature Study," in *Proceedings of the 36th European Photovoltaic Solar Energy Conference and Exhibition (EU PVSEC)*, Marseille, France, 2019, pp. 229–234.

[5] S. De Wolf, A. Descoeudres, Z. C. Holman, and C. Ballif, "High-efficiency Silicon Heterojunction Solar Cells: A Review," *Green*, vol. 2, no. 1, pp. 7–24, 2012, doi: 10.1515/green-2011-0018.

[6] S. K. Chunduri and M. Schmela, "Heterojunction Solar Technology: 2022 Edition," 2022.

[7] B. A. Korevaar, J. A. Fronheiser, X. Zhang, L. M. Fedor, and T. R. Tolliver, "Influence of annealing on performance for hetero-junction a-Si/c-Si devices," in *Proceedings of the 23rd European Photovoltaic Solar Energy Conference and Exhibition*, Valencia, Spain, 2008, pp. 1859–1862.

[8] C. Luderer, C. Messmer, M. Hermle, and M. Bivour, "Transport Losses at the TCO/a-Si:H/c-Si Heterojunction: Influence of Different Layers and Annealing," *IEEE Journal of Photovoltaics*, vol. 10, no. 4, pp. 952–958, 2020, doi: 10.1109/JPHOTOV.2020.2983989.

[9] U. K. Das, M. Z. Burrows, M. Lu, S. Bowden, and R. W. Birkmire, "Surface passivation and heterojunction cells on Si (100) and (111) wafers using dc and rf plasma deposited Si:H thin films," *Appl Phys Lett*, vol. 92, no. 6, p. 63504, 2008, doi: 10.1063/1.2857465.

[10] J. Haschke *et al.*, "Annealing of Silicon Heterojunction Solar Cells: Interplay of Solar Cell and Indium Tin Oxide Properties," *IEEE J. Photovoltaics*, pp. 1–6, 2019.

[11] L. Tutsch *et al.*, "Implementing transparent conducting oxides by DC sputtering on ultrathin SiOx / poly-Si passivating contacts," *Sol Energ Mat Sol C*, vol. 200, pp. 1–5, 2019, doi: 10.1016/j.solmat.2019.109960.

[12] S. Pingel *et al.*, "Low-temperature Ag-Paste Screening for Silicon Heterojunction Solar Cells and Modules," in *Proceedings of the 37th European Photovoltaic Solar Energy Conference and Exhibition (EU PVSEC)*, online, 2020, pp. 508–511.

[13] D. Erath *et al.*, "Fast screen printing and curing process for silicon heterojunction solar cells," in *Proceedings of the 9th Workshop on Metallization and Interconnection for Crystalline Silicon Solar Cells*, Genk, Belgium, 2021, p. 20006.

[14] E. Kobayashi *et al.*, "Increasing the efficiency of silicon heterojunction solar cells and modules by light soaking," *Sol Energ Mat Sol C*, vol. 173, pp. 43–49, 2017, doi: 10.1016/j.solmat.2017.06.023.

[15] A. Moldovan *et al.*, "Improved layer properties combined with light soaking enabling for 23% efficient silicon heterojunction solar cells," in *Proceedings of the 37th European Photovoltaic Solar Energy Conference and Exhibition (EU PVSEC)*, online, 2020, pp. 218–222.

[16] S. De Wolf and M. Kondo, "Nature of doped a-Si:H/c-Si interface recombination," *Journal of Applied Physics*, vol. 105, no. 10, 103707, 2009, doi: 10.1063/1.3129578.

[17] D. Güldali and A. De Rose, "Material Joint Analysis of Lead-Free Interconnection Technologies for Silicon Photovoltaics," in *45th International Spring Seminar on Electronics Technology (ISSE)*, 2022.